Numerical and Experimental Studies of Excitation Force Approximation for Wave Energy Conversion

Bingyong Guo[a], Ron J. Patton[b,*], Siya Jin[b], Jianglin Lan[b]

[a] *College of Engineering Mathematics and Physical Sciences, University of Exeter, Harrison Building, North Park Road, Exeter, UK, EX4 4QF*
[b] *School of Engineering and Computer Science, University of Hull, Cottingham Road, Hull, UK, HU6 7RX*

Abstract

Past or/and future information of the excitation force is useful for real-time power maximisation control of Wave Energy Converter (WEC) systems. Current WEC modelling approaches assume that the wave excitation force is accessible and known. However, it is not directly measurable for oscillating bodies. This study aims to provide accurate approximations of the excitation force for the purpose of enhancing the effectiveness of WEC control. In this work, three approaches are proposed to approximate the excitation force, by (i) identifying the excitation force from wave elevation, (ii) estimating the excitation force from the measurements of pressure, acceleration and displacement, (iii) observing the excitation force via an unknown input observer. These methods are compared with each other to discuss their advantages, drawbacks and application scenarios. To validate and compare the performance of the proposed methods, a 1/50 scale heaving point absorber WEC was tested in a wave tank under variable wave scenarios. The experimental data were in accordance with the excitation force approximations in both the frequency- and time-domains based upon both regular and irregular wave excitation. Although the experimental data were post-processed for model verification, these approaches can be applied for real-time power maximisation control with excitation force prediction.

*Corresponding author
Email addresses: B.Guo@exeter.ac.uk (Bingyong Guo), R.J.Patton@hull.ac.uk (Ron J. Patton), S.Jin@2015.hull.ac.uk (Siya Jin), lanjianglin@126.com (Jianglin Lan)

Keywords: excitation force modelling, model verification, wave energy conversion, system identification, unknown input observer, wave tank tests

1. Introduction

To harvest green power from the ocean waves, more than 1,000 concepts of wave energy conversion have been proposed [1]. Various technologies and devices for wave energy conversion were detailed in [2, 3, 4]. Recent research focuses on the power maximisation control of various Wave Energy Converters (WECs) [5], including reactive control [6], latching control [7], declutching control [8], Model Predictive Control (MPC) [9, 10] and etc. For some of these power maximisation control strategies, the excitation force information is compulsory and essential. Some of these strategies, e.g. MPC, even depend on excitation force prediction. However, the excitation force is not directly measurable for oscillating WECs. Thus, the estimation of the excitation force with reasonable accuracy is critical for some real-time power maximisation control of WEC systems.

In the literature, considering the regular wave conditions, the excitation force was modelled in a generic way using analytical approaches. As described in [11], the excitation force was represented by the integral of the pressure over the wetted surface of a floating structure. This method can give a good estimation of the excitation force but it is not implementable for moving structures in offshore environment. Also for some specific geometries there are appropriate analytical formulae that provide relatively precise excitation force estimation [12]. These approaches assume the phase shift of the excitation force with respect to the incident wave is zero for harmonic waves, thereby rendering these excitation force modelling approaches applicable for numerical WEC simulation. However, these approaches are inappropriate for generating reference information for real-time control implementations since the excitation force is not directly measurable for oscillating structures.

For irregular wave conditions, the excitation force can be approximated using a superposition assumption in terms of the well-known Frequency Response

Function (FRF) [13]. Excitation force estimation is useful for assessing both the wave energy resource as well as the WEC dynamics and control performance. What is the drawback? This approach does not easily relate the excitation force estimation to physical measurements, e.g incident wave elevation or pressure acting on the wetted surface of the oscillating structure. Hence, once again it is difficult to obtain time-varying reference signals for real-time WEC control using this strategy.

However, several studies focused specifically on excitation force estimation or approximation for future real-time control implementation. A state-space modelling method of the causalised excitation force was described in [14] without discussing its realisation and performance. A potential approach to achieve the causalisation with up-stream wave measurement was mathematically discussed in [15] and experimentally verified in [16]. The up-stream method can provide enough future information of the excitation force for some optimum control strategies if the up-stream distance and direction are properly designed to overcome the irregularity of wave frequency and direction. The study in [17] detailed the discrete-time identification of non-linear excitation force based on numerical wave tank simulation. Studies in [18, 19] applied the Kalman Filter (KF) and Extended Kalman Filter (EKF) to estimate the excitation force. However, as discussed in [18, 19] the KF/EKF approaches require a priori knowledge of the process and measurement noises. The measurement noise can be estimated for the characteristics of the sensors and the data acquisition systems whilst the process noise can be obtained from a wide range of specially designed experiments. Also the Unknown Input Observer (UIO) technique was applied to estimate the excitation force in [20, 21]. This approach relies on the accessibility of all the system state variables, some of which are difficult to measure. All these approaches relate the excitation force approximations with real-time wave elevation or/and WEC dynamics and hence the approximations can be used for real-time control reference generation. Moreover, to gain future information of the excitation force for latching control or MPC, Auto-Regressive (AR) or Auto-Regressive-Moving-Average (ARMA) models can be applied to provide short-term prediction of the excitation force, as detailed in [22, 23].

This study aims to develop an excitation force estimation/approximation strategy with potential for real-time WEC power maximisation control. Three approaches are proposed as:

- In the Wave-To-Excitation-Force (W2EF) approach, the excitation force is estimated from the wave elevation. This method is inspired by the causalisation concept in [14] but contributes to its implementation, verification and performance evaluation. The causalisation is achieved via wave prediction using the W2EF method. This can be compared with the up-stream measurement approach of and realised using up-stream wave measurement according to [16]. If the up-stream distance is large enough, the up-stream method can provide enough future information of the excitation force for some power maximisation control strategies, such as MPC and latching control. The W2EF method proposed in this study only gives the current information of the excitation force. However, future information of the excitation force can also be provided by the W2EF method if the wave prediction horizon is large enough. This idea is quite similar to increasing the up-stream distance.

- In the Pressure-Acceleration-Displacement-To-Excitation-Force (PAD2EF) method, the excitation force is derived from the WEC hull pressure measurements and WEC acceleration/displacement in heave. Different from the excitation force identification method using pressure sensors in [16], the PAD2EF approach uses more kinds of sensors and hence has the advantage of sensing redundancy and the disadvantage of system complexity.

- In the Unknown-Input-Observation-of-Excitation-Force (UIOEF) technique, the excitation force is observed from an appropriately designed UIO. Compared to the UIO method in [20, 21], this UIOEF approach only requires the displacement measurement and hence it is more flexible in practice. The UIO design is based on a Linear Matrix Inequality (LMI) formulation of an H_∞ optimisation to minmise the effect of the excitation force derivative on the estimation error.

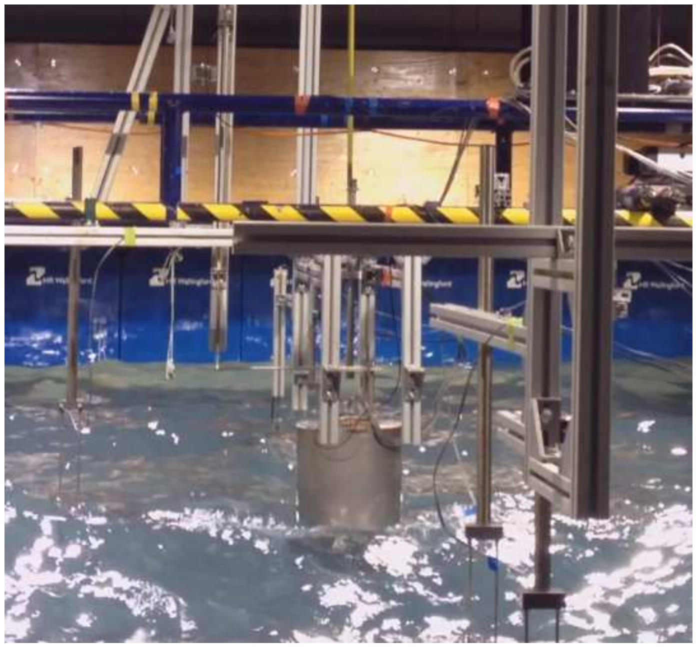

Figure 1: 1/50 scale PAWEC under wave tank test.

Table 1: Dimension of the cylindrical buoy.

Symbol	Parameter	Units	Value
r	buoy radius	m	0.15
h	buoy height	m	0.56
d	buoy draught	m	0.28
M	buoy mass	kg	19.79
k_{hs}	hydrostatic stiffness	N/m	693.43
A_∞	added mass at infinite frequency	kg	6.57

To verify the proposed excitation force modelling approaches, a 1/50 scale cylindrical heaving Point Absorber Wave Energy Converter (PAWEC) was designed, constructed and tested in a wave tank at the University of Hull, as illustrated in Figure 1. The buoy dimensions are given in Table 1. A wide variety of wave tank tests were conducted under regular and irregular wave conditions for verification of the three proposed W2EF, PAD2EF and UIOEF modelling strategies. The experimental data showed a high correspondence with the numerical results of these approaches both in the time- and frequency-domains. Based on the numerical/experimental comarision, the advantages, drawbacks and application scenarios of these approaches are also discussed in this study.

This paper is structured as follows. In Section 2, the modelling of the PAWEC motion is described. Section 3 details the W2EF, PAD2EF and UIOEF approaches to estimate the excitation force in real-time. Section 4 illustrates the wave tank tests configuration and wave conditions of the excitation tests and wave-excited-motion tests. Numerical and experimental results are compared and discussed in Section 5 and conclusions are drawn in Section 6.

2. Modelling of PAWEC Motion

Under the assumptions of ideal fluid (inviscid, incompressible and irrotational), linear wave theory and small motion amplitude, the motion of a PAWEC obeys Newton's second law, given in an analytical representation in [24] as:

$$M\ddot{z}(t) = F_e(t) + F_r(t) + F_{hs}(t) + F_{pto}(t). \tag{1}$$

$F_e(t)$, $F_r(t)$, $F_{hs}(t)$ and $F_{pto}(t)$ are the excitation, radiation, hydrostatic and Power Take-Off (PTO) forces. M is the mass of the PAWEC. $z(t)$ is the heaving displacement and $\ddot{z}$ represents the buoy acceleration in heave. It is assumed that friction, viscous and mooring forces are neglected here. For the sake of simplicity, only the heave motion is investigated in this study.

For a vertical cylinder shown in Figure 1, the hydrostatic force is proportional to the displacement $z(t)$, represented as [25]:

$$F_{hs}(t) = -\rho g \pi r^2 z(t) = -k_{hs} z(t), \tag{2}$$

where ρ, g are the water density and gravity constant, respectively. r and $k_{hs} = \rho g \pi r^2$ represent the buoy radius and hydrostatic stiffness, respectively.

The radiation force $F_r(t)$ is characterised by the added mass and radiation damping coefficient. According to the Cummins equation [26], the radiation force can be written in the time-domain as:

$$F_r(t) = -A_\infty \ddot{z}(t) - k_r(t) * \dot{z}(t), \tag{3}$$

where A_∞ and $k_r(t)$ are the added mass at infinite frequency and the kernel function, or so-called Impulse Response Function (IRF), of the radiation force. $X * Y$ represents the convolution operation of X and Y.

For modelling of the excitation force $F_e(t)$, analytical approaches have been developed in [11, 13]. For regular waves, an analytical representation of the excitation force is given as [11]:

$$F_e(t) = \frac{H}{2} \left(\frac{2\rho g^3 R(\omega)}{\omega^3} \right)^{1/2} \cos(\omega t), \tag{4}$$

where H, ω and $R(\omega)$ represent the wave height, angular frequency and radiation damping coefficient, respectively. For irregular waves, the excitation force can be approximated based on the superposition principle and its FRF, given in a spectrum form in [13], as:

$$F_e(t) = \Re \left[\sum_i \sqrt{2S(\omega_i)\Delta\omega} H_e(j\omega_i) e^{j(\omega_i t + \phi_i)} \right], \tag{5}$$

where $\Delta\omega$ is the angular frequency step, ω_i and ϕ_i are the wave frequency and random phase with subscript i. $S(\omega_i)$ and $H_e(j\omega_i)$ represent the wave spectrum and the excitation force FRF, respectively.

The analytical representations in Eqs. (4) and (5) are widely used to assess the power capture performance of various WEC devices. These may not be suitable for real-time WEC control application since the excitation force is an unknown, uncontrollable and unmeasurable external stochastic input. Hence, the motivation for this study comes from a need to approximate/estimate the excitation force from the given WEC measurements for the purpose of generating suitable reference information for real-time WEC control.

For good WEC control performance, the challenge is that a real-time representation of the excitation force is essential. Therefore, in many studies the Computational Fluid Dynamics (CFD) techniques are adopted to compute the fluid-structure interaction for WEC dynamic modelling. One should recall that the WEC hydrodynamics are non-linear and hence the CFD analysis is computationally expensive. It is actually not straightforward to apply control strategies based on CFD results without very significant effort of CFD data characterisation and post-processing. An effective study that combines control and CFD together based on OpenFOAM simulation was described in [27]. Meanwhile the Boundary Element Method (BEM) packages, such as WAMIT®, AQWA™and NEMOH, are applied to compute the WEC-wave interaction using efficient computation. Amongst these BEM packages, NEMOH is an open source code, dedicated to compute first order wave loads on offshore structures [28]. It is a suitable alternative to commercial BEM codes, like WAMIT® and AQWA™, since it provides computation results as accurate as WAMIT® [29]. Therefore, NEMOH is adopted in this study.

The radiation coefficients in Eq. (3) and the excitation force FRF in Eq. (5) were obtained by solving the boundary value problem in NEMOH [28]. The NEMOH simulation was based on the buoy as shown in Figure 1. The radiation force kernel function $k_r(t)$ is shown in Figure 2 and the excitation force FRF (including the amplitude and phase responses) is shown in Figure 3. In Figure 3 the amplitude response of the excitation force was normalised with respect to the hydrostatic stiffness k_{hs} and the phase response was normalised with respect to π. Since the time-domain representation is preferred for real-time power optimisation control, Section 3 discusses the modelling or approximation approaches of the excitation force.

3. Excitation Force Approximation Approaches

As described in Section 2, the excitation force FRF was obtained from NEMOH. Therefore, a time-domain representation of the excitation force can

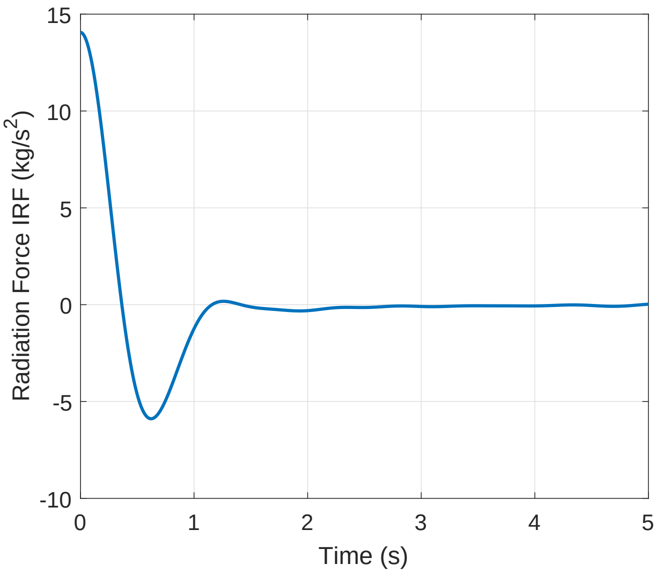

Figure 2: Kernel function of the radiation force from NEMOH.

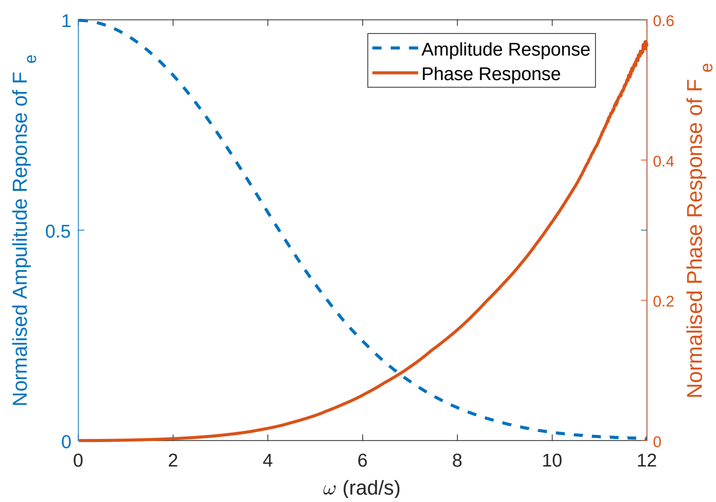

Figure 3: Amplitude and phase responses of the excitation force from NEMOH.

be identified from its FRF if the incident wave is assumed as the input, referred to as the W2EF method. For an oscillating device, if the pressure distribution on the wetted surface and the WEC motion are measurable, the excitation force can be estimated from these measurements as well, referred to as the PAD2EF approach. For some WEC systems, only the oscillating displacement is accessible. In this situation, the excitation force can be estimated via UIO techniques, referred to as the UIOEF method. These approximation approaches of the excitation force are detailed in Sections 3.1, 3.2 and 3.3, respectively.

3.1. W2EF Modelling

3.1.1. Outline of W2EF Method

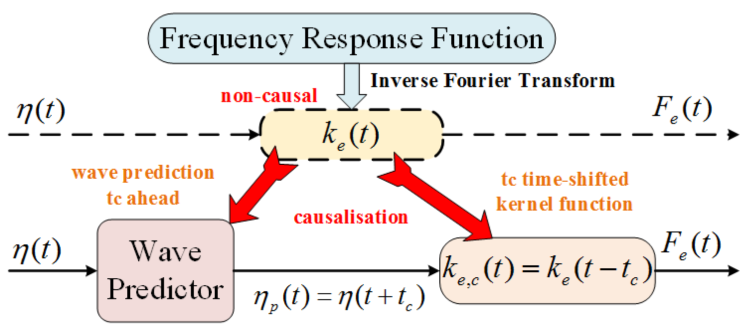

Figure 4: Schematic diagram of the W2EF modelling approach.

Since the frequency-domain response of the excitation force is given in Figure 3, its time-domain kernel function $k_e(t)$ can be gained by the inverse Fourier transform. However, the kernel function $k_e(t)$ characterises that the W2EF process is non-causal. Therefore, a time-shift technique is applied to causalise the non-causal kernel function $k_e(t)$ to its causalised form $k_{e,c}(t)$ (see Figure 4) with causalisation time t_c ($t_c \geq 0$). Thus, the wave elevation prediction with t_c in advance is required. The implementation of the W2EF modelling is detailed in this Section.

According to the frequency-domain response in Figure 3, the excitation force can be represented as:

$$F_e(j\omega) = H_e(j\omega)A(j\omega), \tag{6}$$

where $H_e(j\omega)$ is the FRF of the W2EF process. $A(j\omega)$ is the frequency-domain representation of the incoming wave elevation $\eta(t)$.

Alternatively, the excitation force can be expressed in the time-domain as:

$$F_e(t) = k_e(t) * \eta(t) = \int_{-\infty}^{\infty} k_e(t-\tau)\eta(\tau)d\tau, \tag{7}$$

where $k_e(t)$ is the excitation force IRF related to its FRF $H_e(j\omega)$, given as:

$$k_e(t) = \frac{1}{2\pi}\int_{-\infty}^{\infty} H_e(j\omega)e^{j\omega t}d\omega. \tag{8}$$

Based on the frequency-domain response in Figure 3, the kernel function $k_e(t)$ is computed according to Eq. (8) and shown in Figure 5, in which the red solid curve (marked NEMOH IRF ($t < 0$)) illustrates the non-causality of the W2EF process. The physical meaning of the non-causality was explained in [15]. The $k_e(t)$ values for the $t < 0$ part are almost the same as the $t \geq 0$ part. Therefore, ignoring of the non-causality will in general lead to significant errors in the excitation force estimation.

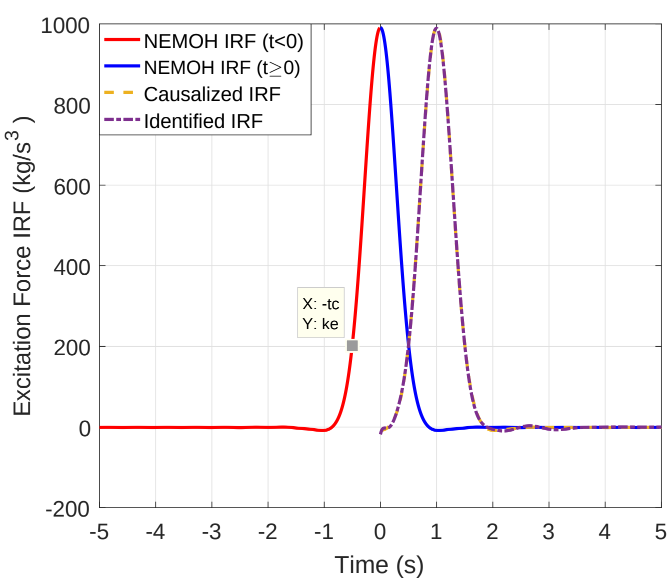

Figure 5: Comparison of the excitation force IRFs.

To note: In [14, 15], the kernel function $k_e(t)$ was time-shifted first and then treated as a curve fitting problem. However, the implementation procedure and the results of the excitation force were not given in [14, 15]. In this study, both the causalisation and its implementation with wave prediction are outlined in this Section. The numerical and experimental results of the excitation force are compared in both the time- and frequency-domains in Section 5.1.

As shown in Figure 4, the incident wave propagates through a non-causal system characterised by $k_e(t)$ and gives the excitation force approximation. However, this non-causal system is not implementable. Therefore, causalisation is required and can be achieved with a time-shifted kernel function $k_{e,c}(t)$ and wave prediction $\eta_p(t)$. The wave prediction horizon is the same as the causalisation time t_c.

According to the property of the convolution operation, this causalised system with wave prediction gives the same excitation force of the non-causal system [14], since:

$$F_e(t) = k_e(t) * \eta(t) \tag{9}$$

$$= k_e(t - t_c) * \eta(t + t_c) \tag{10}$$

$$= k_{e,c}(t) * \eta_p(t), \tag{11}$$

where

$$k_{e,c}(t) = k_e(t - t_c), \tag{12}$$

$$\eta_p(t) = \eta(t + t_c). \tag{13}$$

$k_{e,c}(t)$ and $\eta_p(t)$ are the causalised IRF of the excitation force and the predicted wave elevation with t_c in advance, respectively. The procedures to identify the $k_{e,c}(t)$ and to predict the $\eta_p(t)$ are detailed as follows.

3.1.2. System Identification of Causalised Kernel Function

The excitation force expressed in Eq. (11) is causal if the predicted wave is viewed as the system input. Hence, the convolution operation can be approximated by a finite order system [14, 29, 30]. In this study, realisation theory is applied to the causalised kernel function $k_{e,c}(t)$ to approximate the system matrices in Eqs. (14) and (15) directly with the MATLAB® function *imp2ss* [31] from the robust control toolbox. The order number of the identified system is quite high, as determined by $k_{e,c}(t)$. Hence, model reduction is required and achieved using the square-root balanced model reduction method with MATLAB® function *balmar* [32].

In this study Eq. (11) is approximated by the following state-space model:

$$\dot{x}_e(t) = A_e x_e(t) + B_e \eta_p(t), \quad (14)$$

$$F_e(t) \approx C_e x_e(t), \quad (15)$$

where $x_e(t) \in \mathbb{R}^{n\times 1}$ is the state vector for the excitation system. $A_e \in \mathbb{R}^{n\times n}$, $B_e \in \mathbb{R}^{n\times 1}$ and $C_e \in \mathbb{R}^{1\times n}$ are the system matrices. n represents the system order number.

To identify the causalised system, the causalisation time t_c and the system order number n should be selected carefully. Here a truncation error function E_t is defined to evaluate the causalisation time, given as:

$$E_t = \frac{\int_{-\infty}^{-t_c} |k_e(t)|dt}{\int_{-\infty}^{\infty} |k_e(t)|dt}. \quad (16)$$

For $t_c \in [0, 5]$, the truncation error is given in Figure 6. For $t_c = 0.8$ s, the truncation error was about $E_t = 0.0104$ and for $t_c = 2$ s, the truncation error was about $E_t = 0.0044$. Increasing the causalisation time can decrease the truncation error. However, the truncation error was small enough for $t_c \in [0.8, 2]$. Thus $t_c = 0.8 : 0.05 : 2$ s was selected to determine the system order number n.

To further determine the causalisation time t_c and the system order n, a fitting-goodness function (defined as FG) of the causalised IRF $k_{e,c}(t)$ is defined with a cost-function of Normalized Mean Square Error (NMSE), as:

$$FG = 1 - \left\| \frac{x_{ref} - x}{x_{ref} - \bar{x}_{ref}} \right\|_2^2, \quad (17)$$

where $\|X\|_2^2$ and $\bar{X}$ are the 2-norm and mean value of vector X, respectively. The fitting-goodness tends to 1 for the best fitting and $-\infty$ for the worst fitting.

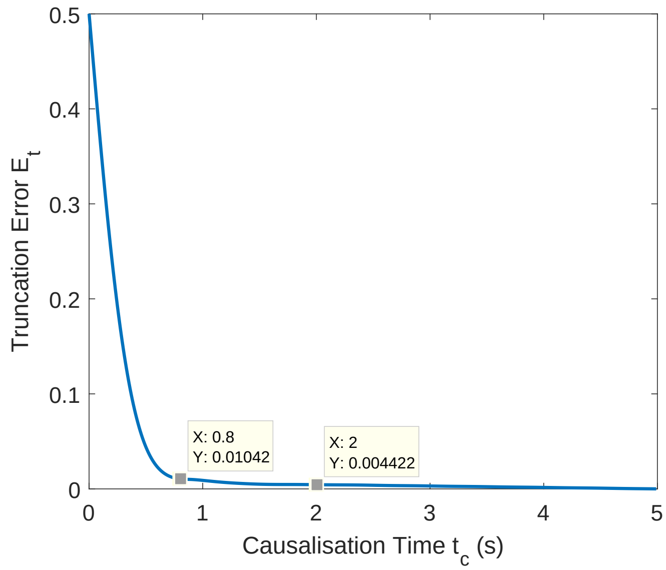

Figure 6: Truncation error of the excitation force IRF varies against the causalisation time.

The fitting-goodness of the causalised excitation IRF relies on the causalisation time t_c and system order number n. Figure 7 shows the fitting-goodness function varying with the caulisation time $t_c = 0.8 : 0.05 : 2$ s and the system order number $n = 3 : 1 : 8$. For a constant t_c, the fitting-goodness increased as the system order number n increased. To achieve a perfect fitting or identification (such as a given fitting-goodness $FG \geq 0.98$), a larger causalisation time requires a higher system order number n. For instance, $n = 4$ gave $FG \geq 0.98$ for $t_c = 1$ s and $n = 5$ was requred to achieve $FG \geq 0.98$ for $t_c = 1.2$ s.

According to Figures 6 and 7, a system with $t_c = 1$ s and $n = 6$ can give a low truncation error ($E_t < 0.01$) and a good fitting of the causalised kernel function $k_{e,c}(t)$ ($FG > 0.99$). Hence $t_c = 1$ s and $n = 6$ were selected for this study. The identified IRF is compared with the causalised and original IRFs of the excitation force in Figure 5. Note that $t_c = 1$ s was selected here to overcome the non-causality of the W2EF process and to provide current information of the excitation force. Future information of the excitation force can be obtained

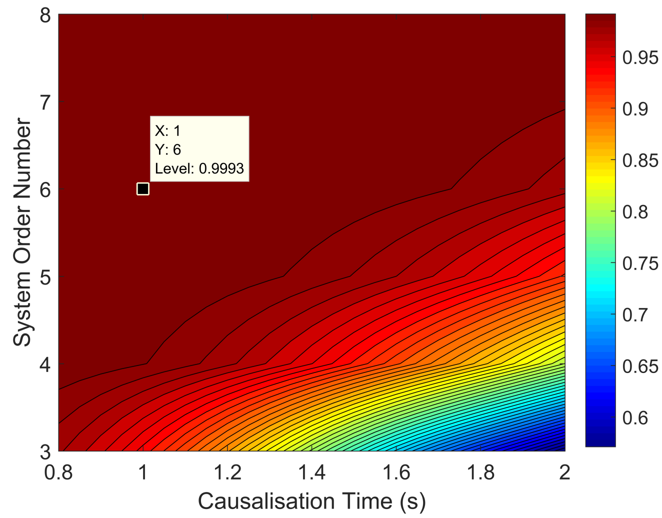

Figure 7: Fitting-goodness with varying causalisation time t_c and system order number n.

via excitation force prediction or increasing the wave prediction horizon.

3.1.3. Wave Prediction

According to Eq. (10), a short-term wave prediction is required to achieve the causalisation problem in Figure 4. There are several approaches to provide reasonably accurate wave predication for a short-term horizon, the most note worthy of which are: (i) the AR model approach [22], (ii) the ARMA model approach [23] and (iii) the fast Fourier transform approach [33]. The real-time implementation of wave prediction was discussed in [34]. In [22], wave prediction via AR model showed a high accordance to the ocean waves in Irish sea. Since these techniques are mature, the AR model approach developed in [22] was adopted in this study to provide a short-term wave prediction.

For harmonic waves, wave prediction is easy to achieve. For irregular waves, three campaigns of wave prediction practice using AR model are shown in Figure 8. The wave elevation $\eta(t)$ was acquired from wave tank tests and satisfied the Pierson-Moskowitz (PM) spectrum [35] with peak frequency $f_p = 0.4$, 0.6, 0.8 Hz. As suggested in [22], a low-pass filter was applied to the wave elevation measurements for improving the prediction performance. The wave prediction horizon was the same as the causalisation time t_c (expressed in Eq. (10)). According to Figure 7, $t_c = 1$ s was selected for the excitation force approximation.

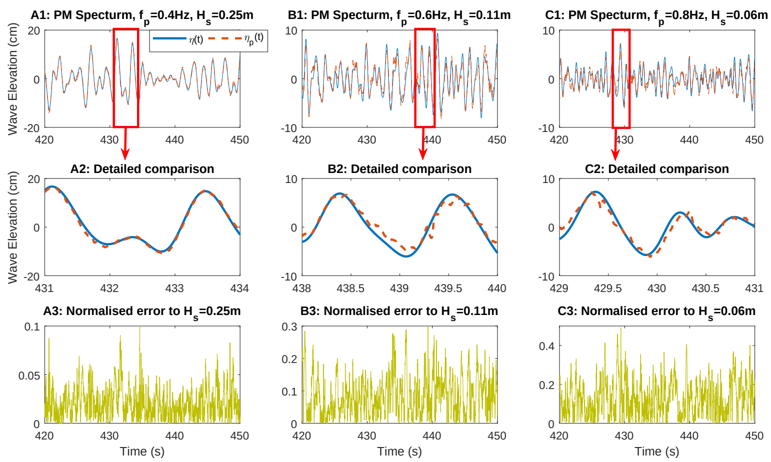

Figure 8: Comparison of wave elevations between the experimental measurements and the numerical predictions under irregular wave conditions. The prediciton errors are normalised with respect to their significant wave heights respectively.

For wave tank tests, the sampling frequency was 100 Hz and hence the prediction horizon was 100 for $t_c = 1$ s. The AR model order number is determined by the goodness-of-fit index defined in [22] and hence the order number was selected as 120 to keep the goodness-of-fit index larger than 70%. The order number is large due to the high sampling frequency and hence it can be reduced by decreasing the sampling frequency. For each campaign of wave tank tests, the experimental data of 600 s were collected and divided into two parts equally. The first part of data ($t = 0 : 0.01 : 300$ s) were used to estimate the AR model parameters and the second part of data ($t = 300 : 0.01 : 600$ s) were used for model verification. This study focuses on the verification of the W2EF method and the AR model parameters were computed off-line. However, the real-time on-line wave prediction can be achieved with embedded systems [34]. Figure 8 indicates that the predicted wave elevation fits the experimental data well and that the prediction performance decreases as the peak frequency increases. For the PM spectrum, a higher peak frequency results in a wider bandwidth and hence one potential way to improve the prediction performance is to increase the order of the AR model when the peak frequency is high. In this study the AR model was adopted as a wave predictor (see Figure 4) to provide future information for the identified system.

3.2. PAD2EF Modelling

3.2.1. Outline of PAD2EF Method

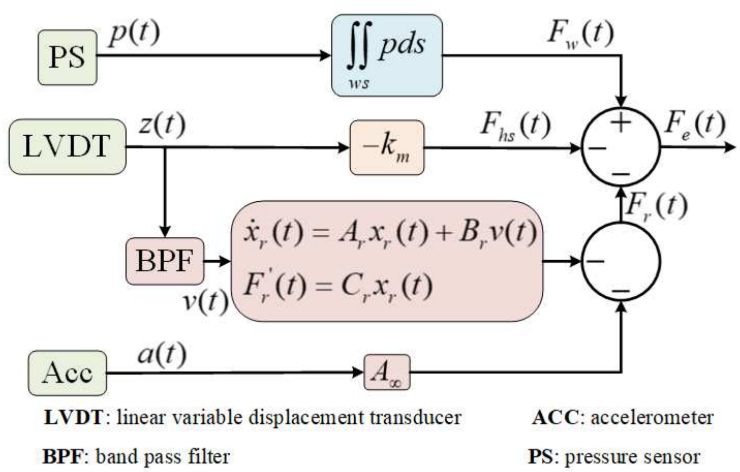

Figure 9: Schematic diagram of the PAD2EF modelling approach.

For an oscillating PAWEC, the excitation force can be reconstructed from its sensing system. As shown in Figure 9, the total wave force $F_w(t)$ acting on the structure can be estimated from the pressure measurement $p(t)$ on the wetted surface. The hydrostatic force defined in Eq. (2) can be represented by the displacement measurement $z(t)$. The radiation force can be approximated from the measurements of the velocity $\dot{z}(t)$ and acceleration $\ddot{z}(t)$. The acceleration measurement is post-processed with a low-pass filter since this study focuses on the PAD2EF method verification rather than its real-time realisation. Therefore, the excitation force can be approximated as:

$$F_e(t) = F_w(t) - F_{hs}(t) - F_r(t). \tag{18}$$

The convolution term of the radiation force $F_r(t)$ in Eq. (3) is approximated by a finite order system [30] as follows.

3.2.2. Radiation Force Approximation

The convolution operation of the radiation force in Eq. (3) is defined as a radiation subsystem, given as:

$$F_r^{'}(t) = k_r(t) * \dot{z}(t). \tag{19}$$

The kernel function $k_r(t)$ was gained from NEMOH and shown in Figure 2. The convolution approximation approach is the same as described in Section 3.1.2.

To determine an appropriate system order number, the fitting-goodness function in Eq. (17) is applied. A third order system was adopted to approximate the radiation subsystem in Eq. (19) with a fitting-goodness of $FG = 0.9989$, as:

$$\dot{x}_r(t) = A_r x_r(t) + B_r \dot{z}(t), \tag{20}$$

$$F_r^{'}(t) \approx C_r(t) x_r(t), \tag{21}$$

where $x_r(t) \in \mathbb{R}^{3\times1}$ is the state vector for the radiation system. $A_r \in \mathbb{R}^{3\times3}$, $B_r \in \mathbb{R}^{3\times1}$ and $C_r \in \mathbb{R}^{1\times3}$ are the system matrices. Therefore, the excitation force can be estimated from the measurements of the pressure, acceleration and displacement, given as:

$$F_e(t) = \iint p(t)ds + k_{hs}z(t) + A_\infty \ddot{z}(t) + F_r^{'}(t). \tag{22}$$

3.2.3. Pseudo-Velocity Measurement

As shown in Figure 9, the measurements of the pressure, displacement and acceleration are accessible and implementable. However, the velocity measurement is difficult and expensive to obtain. A "pseudo-velocity" can be estimated/observed from the displacement/acceleration measurements. In [19], the velocity was obtained from the first order derivative of an accurate displacement measurement with a high sampling frequency. The drawbacks of this approach are: (i) the velocity estimation is corrupted by the measurement noise and (ii) the velocity estimation is always one sample period behind the real velocity (high sampling frequency is required).

In this work, a carefully designed Band-Pass Filter (BPF) was applied to obtain the velocity estimate from the displacement measurement. Compared with the differentiation approach, a velocity estimate with less phase lag can be gained via the BPF. The second order BPF is given as:

$$BPF(s) = \frac{A_{bpf}\frac{\omega_c}{Q_{bpf}}s}{s^2 + \frac{\omega_c}{Q_{bpf}}s + \omega_c^2}, \tag{23}$$

where A_{bpf} is the amplitude gain at the central frequency ω_c and Q_{bpf} is the quality factor. The drawbacks of this BPF method are: (i) the velocity estimation is influenced by measurement noise and (ii) the BPF is difficult to implement with analogue filter. However, the BPF is applicable in a software digital filtering way. Additionally, the velocity can be observed via an appropriately designed observer and this part of work is detailed in Section 3.3.3.

A variety of wave tank tests were conducted under irregular wave conditions and the comparison of the pseudo-velocity measurements between the differential, BPF and observation methods is given in Figure 10. The pseudo-velocity measurements via these three methods showed a high accordance to each other due to: (i) the sampling frequency (100 Hz) is very large compared with the wave frequency (1.2 Hz) and (ii) the displacement measurement is accurate enough. The differential method requires a high sampling frequency and accurate displacement measurement. The BPF approach calls for large A_{bpf} and Q_{bpf} and this may result in instability of the closed-loop control system. The third method of observing the velocity is preferred since the observer design is easy, robust and flexible to implement.

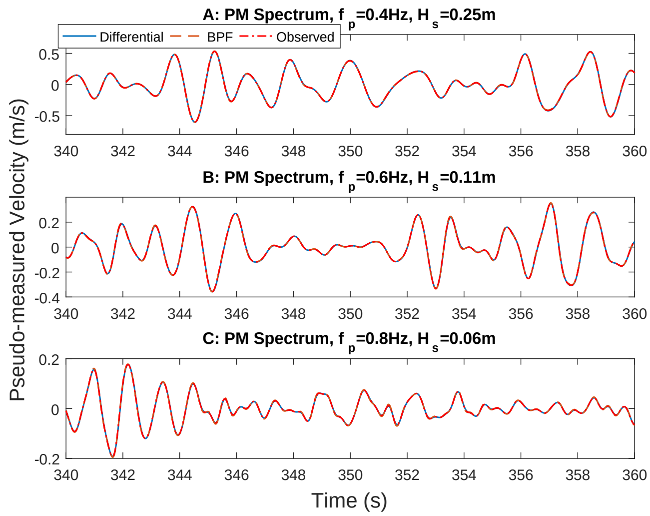

Figure 10: Comparison of pseudo-measured velocity under irregular wave conditions.

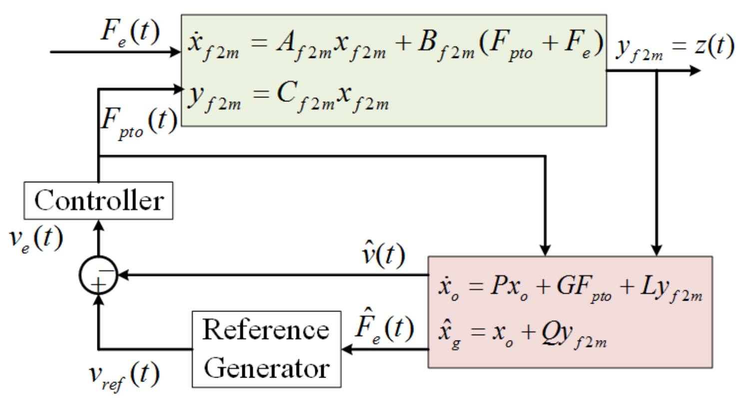

Figure 11: Schematic diagram of the UIOEF modelling approach.

3.3. UIOEF Modelling

3.3.1. Outline of UIOEF Method

As the convolution term of the radiation force in Eq. (19) is approximated by a state-space model in Eqs. (20) and (21), the PAWEC motion under the wave excitation can be represented in a state-space form. Therefore, an appropriately designed UIO can be applied to estimate the unknown excitation force. As shown in Figure 11, a generic UIO is applied to estimate the excitation force and buoy velocity from the displacement measurement. The estimated excitation force is used to generate the velocity reference, whilst the estimated velocity is viewed as the velocity measurement to provide feedback for the controller. However, this study focuses on the UIO estimator design rather than on the controller structure and design. This method is referred to as the UIOEF modelling method.

3.3.2. Force-To-Motion Modelling

According to Eq. (1), the PAWEC starts to oscillate under the stimulation of the excitation and PTO forces. The PAWEC motion with excitation force input is defined as the Force-To-Motion (F2M) model. Considering the radiation approximation in Eqs. (20) and (21), the F2M model is re-written as:

$$x_{f2m} = [z \quad \dot{z} \quad x_r]^T, \tag{24}$$

$$\dot{x}_{f2m}(t) = A_{f2m}x_{f2m}(t) + B_{f2m}F_e(t) + B_{f2m}F_{pto}(t), \tag{25}$$

$$y_{f2m}(t) = C_{f2m}x_{f2m}(t), \tag{26}$$

with

$$A_{f2m} = \begin{bmatrix} 0 & 1 & 0 \\ -\frac{k_{hs}}{M_t} & 0 & -\frac{C_r}{M_t} \\ 0 & B_r & A_r \end{bmatrix}, \tag{27}$$

$$B_{f2m} = \begin{bmatrix} 0 & -\frac{1}{M_t} & 0 \end{bmatrix}^T, \tag{28}$$

$$C_{f2m} = \begin{bmatrix} 1 & 0 & 0 \end{bmatrix}, \tag{29}$$

where $M_t = M + A_\infty$ represents the total mass. $x_{f2m}(t) \in \mathbb{R}^{5\times1}$ is the F2M state vector. $A_{f2m} \in \mathbb{R}^{5\times5}$, $B_{f2m} \in \mathbb{R}^{5\times1}$ and $C_{f2m} \in \mathbb{R}^{1\times5}$ are the system matrices.

3.3.3. Unknown Input Observer Design

The estimator of the unknown excitation force $F_e(t)$ is constructed as an augmented state system. The system given by Eqs. (25) and (26) is augmented to include the wave estimation force $F_e(t)$ as follows:

$$x_g = [x_{f2m} \quad F_e]^T, \tag{30}$$

$$\dot{x}_g(t) = A_g x_g(t) + B_g F_{pto}(t) + D_g \dot{F}_e, \tag{31}$$

$$y_g(t) = C_g x_g(t), \tag{32}$$

with

$$A_g = \begin{bmatrix} A_{f2m} & B_{f2m} \\ 0 & 0 \end{bmatrix}, \tag{33}$$

$$B_g = \begin{bmatrix} B_{f2m} & 0 \end{bmatrix}^T, \tag{34}$$

$$D_g = \begin{bmatrix} 0 & 1 \end{bmatrix}^T, \tag{35}$$

$$C_g = \begin{bmatrix} C_{f2m} & 0 \end{bmatrix}, \tag{36}$$

where $x_g(t) \in \mathbb{R}^{6\times1}$ is the state vector of the augmented system. $A_g \in \mathbb{R}^{6\times6}$, $B_g \in \mathbb{R}^{6\times1}$, $D_g \in \mathbb{R}^{6\times1}$ and $C_g \in \mathbb{R}^{1\times6}$ are the system matrices.

The following UIO is adapted from [36, 37] to estimate the augmented system state, given as:

$$\dot{x}_o(t) = P x_o(t) + G F_{pto}(t) + L y_{f2m}(t), \tag{37}$$

$$\hat{x}_g(t) = x_o(t) + Q y_{f2m}(t), \tag{38}$$

where $x_o(t) \in \mathbb{R}^{6\times1}$ is the UIO state vector. $P \in \mathbb{R}^{6\times6}$, $G \in \mathbb{R}^{6\times1}$, $L \in \mathbb{R}^{6\times1}$ and $Q \in \mathbb{R}^{6\times1}$ are the UIO system matrices. $\hat{x}_g(t)$ represents the estimate of $x_g(t)$.

Since the excitation force is unknown, its derivative $\dot{F}_e(t)$ in Eq. (31) is inaccessible and hence viewed as a disturbance. To achieve an accurate estimation

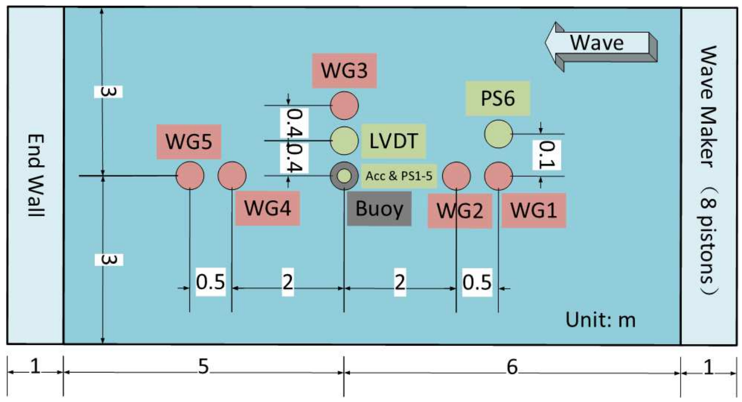

Figure 12: Sketch of the wave tank and the device installation.

of the excitation force, the procedure of H_∞ robust optimisation is used to compute the observer matrices P, G, L and Q to reject the influence of $\dot{F}_e(t)$, using the MATLAB® LMI toolbox. The computation of the observer gain matrix L follows the method described in [37] and is thus omitted here.

4. Wave Tank Tests

4.1. Experiment Settings

To verify the excitation force estimation via the W2EF, PAD2EF and UIOEF approaches, a series of wave tank tests were conducted. As shown in Figure 12, the wave tank was 13 m in length, 6 m in width and 2 m in height (with water depth 0.9 m). Up to 8 pistons can be selected to generate regular/irregular waves.

The PAWEC was scaled down according to the Froude Number defined in [25]. For this application the geometric ratio was selected as 1/50. Therefore, the time ratio was 1/7.0711. For ocean waves of sea state 7 defined by the Beaufort scale [38], its characteristics can be represented by a PM spectrum with peak frequency $f_p = 0.095$ Hz and significant wave height $H_s = 4.3$ m. The scaled down PM spectrum (according to the Froude Number) was featured by the peak frequency $f_p = 0.0952 \times 7.0711 = 0.67$ Hz and significant wave height $H_s = 4.3/50 = 0.086$ m. Therefore, the wave conditions in the wave tank tests were configured with wave frequencies of $f = 0.4 : 0.1 : 1.2$ Hz and a wave height considered as $H = 0.08$ m for regular waves. For irregular waves, the peak frequencies of the PM spectra were selected as $f_p = 0.4, 0.6, 0.8$ Hz.

The 1/50 scale cylindrical heaving PAWEC was simulated, designed and constructed for wave tank tests, model verification and control system design, as shown in Figure 12. Five Wave Gauges (WGs) were mounted to measure the water elevation in real-time, with WG1&2 in the up-stream, WG3 in line with the buoy and WG4&5 in the down-stream. For this study, only the WG3 measurement was used. WG1&2 and WG4&5 were useful to estimate the reflection of the wave tank end wall and to verify the generated irregular wave satisfying the pre-set PM spectrum. Six Pressure Sensors (PSs) were applied in the wave tank tests with PS1-5 installed at the bottom of the PAWEC to measure the dynamic pressure acting on the hull and PS6 fixed in line with WG1 for synchronisation[1]. A Linear Variable Displacement Transducer (LVDT) and a 3-axis Accelerometer (Acc) were rigidly connected with the oscillating body to provide motion measurements. All these sensing signals were collected by a data acquisition system connected with LABVIEW™ panel. The sampling frequency was 100 Hz. The pressure, displacement and acceleration measurements were post-processed with low-pass filters to verify the modelling and estimation concepts. The infinite imulse response low-pass filters were adopted with passband frequency 3 Hz, passband riple 0.2 dB, stopband attenuation 60 dB and order number 10.

For the *excitation tests*, the PAWEC was fixed semi-submerged and under

[1]The installation depth of PS6 was 0.4 m. Two sensing systems were applied: one integrated with the wave maker and the other designed for the PAWEC. An isolation system was made between the two sensing systems to minimise compatibility conflicts. The PAWEC sensing system triggered the wave maker sensing system. However, there was still a small time shift between these two sensing systems due to different design of the hardware and software. Thus PS6 and WG1 were installed to measure the same signal to determine the time shift between these two sensing systems.

the excitation of incident waves to verify the W2EF modelling approach. For the *wave-excited-motion tests*, the buoy was initially set free at its equilibrium point and then was stimulated to oscillate under the excitation of incoming waves. Since this study has a specific focus on the estimations of the excitation force, the control or PTO force was set as $F_{pto} = 0$ N for the excitation tests or the wave-excited-motion tests. For control practice, F_{pto} is known and hence it is applicable to obtain the excitation force by subtracting F_{pto} from the estimate of PAD2EF or UIOEF approaches. If F_{pto} is not known, only the W2EF method is applicable.

4.2. Excitation Tests

For the excitation tests, the PAWEC was fixed to the wave tank gantry at its equilibrium point and excited by the incident wave. The pressure sensors installed at the bottom of the buoy can provide the measurement of the dynamic pressure acting on the hull. Thus, the wave excitation force in heave can be represented as:

$$F_e(t) = \iint p(t)ds \approx \pi r^2 \bar{p}(t), \tag{39}$$

where $\bar{p}(t)$ represents the average value of the five pressure sensors (PS1-5). Note that Eq. (39) only gives an simple approximation of the the excitation force. When the buoy diameter is relatively small compared with the wavelength (such as tenth of the wavelength), the accuracy of Eq. (39) is acceptable. If the buoy dimension is almost the same scale of the wavelength, more pressure sensors are required to achieve accurate excitation force measurement.

Meanwhile, five WGs were installed to measure the wave elevation, amongst which, WG3, was in line with the buoy. The measurement of WG3 represented the incident wave at the center of the PAWEC and was adopted to provide wave prediction in a short-term horizon t_c. A wide variety of excitation tests under regular and irregular wave conditions were conducted to verify the W2EF modelling approach. The numerical and experimental results are compared and discussed in Section 5.1.

4.3. Wave-Excited-Motion Tests

For the wave-excited-motion tests, the PAWEC was initially set free at its equilibrium point (zero-initial condition) and then was stimulated to oscillate under the excitation of incident waves. In this situation, the measurements from pressure sensors represent the total wave force rather than the excitation force, given as:

$$F_w(t) = \iint p(t)ds \approx \pi r^2 \bar{p}(t). \tag{40}$$

Also, Eq. (40) is valid only when the buoy dimension is relatively small compared with the wavelength.

Meanwhile, the buoy acceleration and displacement were measured by the accelerometer and LVDT, respectively. Therefore, the excitation force can be estimated via the PAD2EF approach in Eq. (22). Also, the wave elevation measurements were accessible. Thus the W2EF method can be applied on WG3 measurement to approximate the excitation force according to Eqs. (14) and (15). Since the displacement measurement was accessible, the UIOEF approach in Eqs. (37) and (38) can be applied to estimate the excitation force as well. The numerical and experimental comparison of the excitation force between the W2EF, PAD2EF and UIOEF approaches is discussed in Section 5.2.

5. Results and Discussion

5.1. Results of Excitation Tests

Since the PAWEC was fixed during the excitation tests. The motion measurements were not applicable. Therefore, only the W2EF approach can be applied to estimate the excitation force. To verify the proposed W2EF modelling approach, excitation tests were conducted under regular and irregular wave conditions and the experimental data were compared with the numerical simulations of Eqs. (14) and (15).

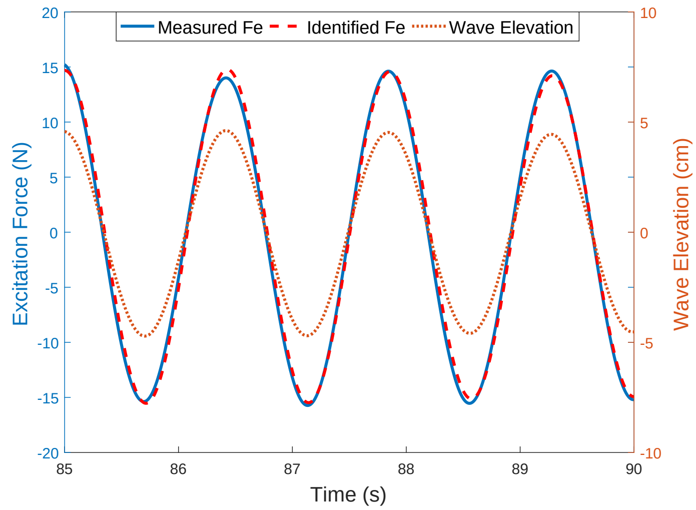

Figure 13: Comparison of the excitation forces between the measurement and the estimate via W2EF method.

5.1.1. Regular Wave Conditions

Nine excitation tests were conducted under regular waves with wave height $H = 0.08$ m and frequencies $f = 0.4 : 0.1 : 1.2$ Hz. For harmonic waves, precise wave prediction with horizon $t_c = 1$ s is easy to achieve. Recall that the prediction horizon is the same as the causalisation time illustrated in Eq. (10) and Figure 7. Therefore, the W2EF modelling approach can always provide accurate approximation of the excitation force under regular waves. For the harmonic wave with frequency $f = 0.7$ Hz, the excitation force measurement in Eq. (39) and the estimation in Eqs. (14) and (15) are compared in Figure 13. The estimation via W2EF method showed a high accordance with the experimental data, which indicates the validity of the W2EF method for excitation tests under regular wave conditions.

To check the fidelity further, the excitation force FRF was compared with the W2EF result as well as with the NEMOH computation. The amplitude and phase responses are shown in Figures 14 and 15, respectively. The amplitude response of the W2EF method fitted the NEMOH and excitation tests data to a high degree. This is why the analytical representations of the excitation force in Eqs. (4) and (5) are widely adopted to investigate WEC dynamics. Note that the excitation force amplitude response was normalised with respect to the hydrostatic stiffness k_{hs}.

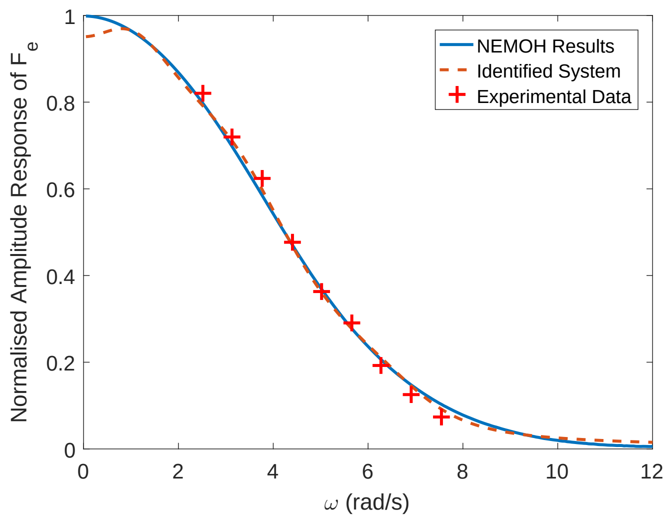

Figure 14: Amplitude response comparison of the excitation force amongst the excitation tests, NEMOH computations and W2EF simulations.

Figure 15 compares the experimental and numerical phase responses from the incident wave $\eta(t)$ to the excitation force $F_e(t)$ in Eq. (9). A good accordance of the phase response means that the W2EF modelling approach with kernel function causlisation and wave prediction in Eq. (11) gives almost the same system description of the non-causal system in Eq. (9). Also, Figure 15 illustrates that the analytical representations of the excitation force in Eq. (4) is improper for PAWEC modelling and control design since the phase response is ignored, especially when the wave frequency is relatively high. Note that, the excitation force phase response was normalised with respect to π.

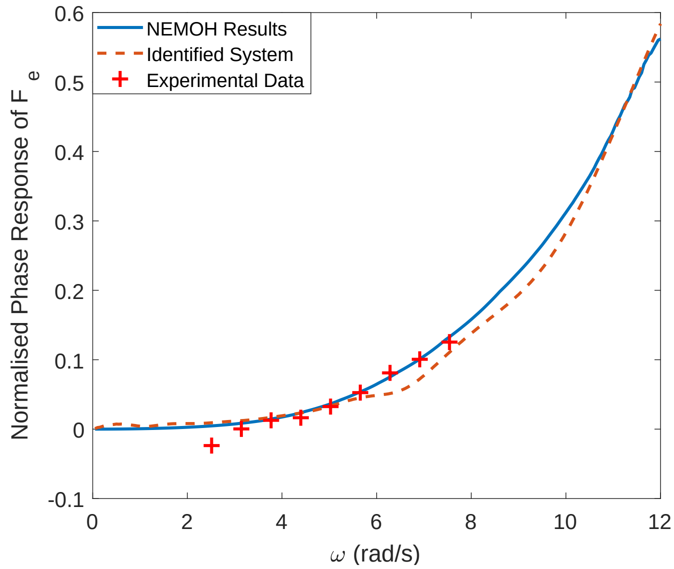

Figure 15: Phase response comparison of the excitation force amongst the excitation tests, NEMOH computations and W2EF simulations.

5.1.2. Irregular Wave Conditions

Irregular waves characterised by the PM spectrum were adopted in the excitation tests and the results are shown in Figure 16. Generally speaking, the estimated excitation force via the W2EF method showed a good accordance to the experimental data for most of the time. The estimation varied only slightly from the measurement when the wave elevation was occasionally small. For instance, the identified excitation force varied from its measurement for $t \in [436, 440]$ s in Figure 16, case A. However, this part was not important from the viewpoint of power maximisation. For the irregular wave condition of $f_p = 0.8$ Hz, $H_s = 0.06$ m, the excitation force estimate was not as accurate as that for the other two wave conditions. The potential reason may be the inaccuracy in Eq. (39) since the point absorber assumption are not fully satisfied. Additionally, the wave elevation predictions corresponding to Figure 16 are given in Figure 8.

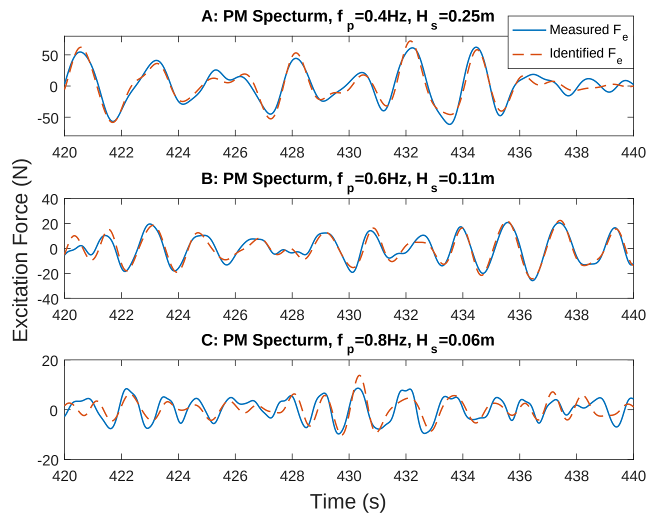

Figure 16: Comparison of the excitation force between the excitation tests and the W2EF modelling under irregular wave conditions.

5.2. Results of Wave-Excited-Motion Tests

For the wave-excited-motion tests, the PAWEC oscillated under the excitation of incident waves. Therefore, the pressure, displacement and acceleration measurements, together with the wave elevation, were available. Thus the W2EF, PAD2EF and UIOEF approaches were adopted to approximate the excitation force acting on the PAWEC hull. In the wave-excited-motion tests, the excitation force was immeasurable since the pressure sensors gave the total wave force $F_w(t)$ in Eqs. (18) and (40).

Three campaigns of wave-excited-motion tests were conducted under irregular wave conditions and the excitation force comparison among the W2EF, PAD2EF and UIOEF approximation approaches is given in Figure 17. Since the excitation force cannot be measured directly, it is very hard to say which method is better. The comparison in Figure 17 indicates that: (i) All these three methods can give good estimation of the excitation force when the wave (or excitation force) was large for the wave conditions of $f_p = 0.4$ Hz, $H_s = 0.25$ m and $f_p = 0.6$ Hz, $H_s = 0.11$ m. (ii) When the wave was small or changed rapidly,

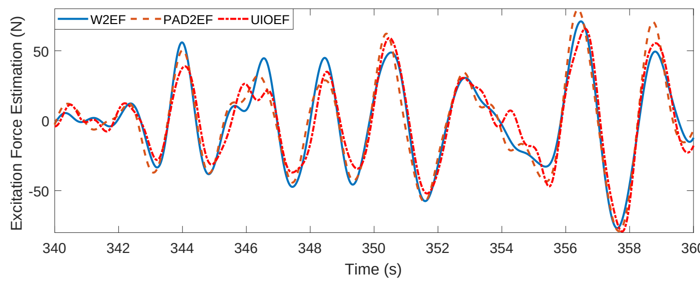

(a) PM spectrum, $f_p = 0.4$ Hz, $H_s = 0.25$ m.

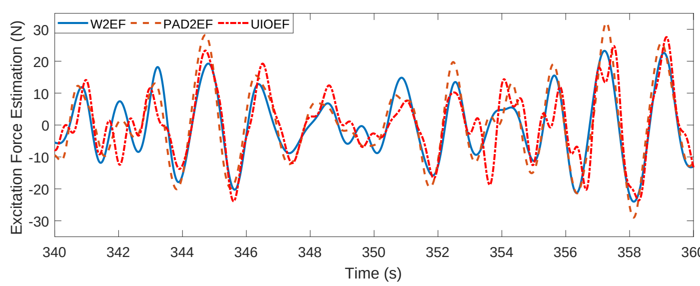

(b) PM spectrum, $f_p = 0.6$ Hz, $H_s = 0.11$ m.

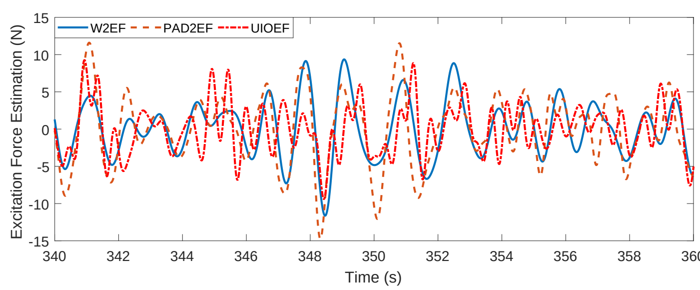

(c) PM spectrum, $f_p = 0.8$ Hz, $H_s = 0.06$ m.

Figure 17: Comparison of the excitation force approximations under irregular wave conditions.

the estimations given by the PAD2EF and UIOEF approaches were more variable, compared with the W2EF estimation. Compared to the excitation force, the radiation approximation error and non-linear friction/viscous forces [39] are relatively large. (iii) Generally speaking, the magnitude of the excitation force approximation given by the W2EF method was smaller than the ones provided by the PAD2EF and UIOEF approaches. One potential reason is that the wave gauge measurement is attenuated by the interference between the incident and radiated waves [16]. (iv) For the wave condition of $f_p = 0.8$ Hz, $H_s = 0.06$ m, the W2EF method gave slightly better estimation than the PAD2EF and UIOEF approaches. One potential reason is that the wave excitation force is small under this wave condition and hence the mechanical friction force is relatively large. The PAD2EF and UIOEF methods in this work cannot decouple the mechanical friction force from there excitation force estimations. For the specified 1/50 PAWEC, the friction can be characterised experimentally [40, 39]. Whilst the W2EF method estimates the wave excitation force from wave measurements and hence the estimates are not affected by mechanical friction force.

A comparison of these methods are made as follows:

- The W2EF modelling approach requires the wave elevation measurement only. The W2EF approach shows advantages in easy implementation and good tolerance to the mechanical friction and fluid viscous forces. However, the W2EF approach is subjected to linear wave theory and small radiated wave. Additionally, accurate wave prediction is compulsory to overcome the non-causality of the W2EF process.

- The PAD2EF modelling method requires the measurements of pressure, acceleration and displacement. Hence it is complex to implement. The PAD2EF estimation is affected by the modelling error of the radiation force approximation and fluid viscous force but not the mechanical friction force and radiated wave. Another advantage is that the PAD2EF estimation is applicable when the incident waves are non-linear or when the W2EF process is non-linear.

- The UIOEF modelling approach only requires the displacement measurement. Thus it is easy to implement. Also, the UIOEF estimation does not suffer from the radiated wave but is influenced by modelling error of the radiation force approximation, the mechanical friction and fluid viscous forces. Also, the UIOEF method can be applied under the excitation of non-linear incident waves.

For the control structure in Figure 11, the estimation error of the excitation force will affect the power capture performance. This part of work was investigated in [41] and it reported that the influence of the estimation error on the power capture can be attenuated at certain band of frequencies via robust control design.

6. Conclusion

This study focuses on the modelling of the excitation force and the model verification via wave tank tests. The excitation force can be approximated with reasonable accuracy from the measurements of wave elevation, pressure, acceleration and displacement. Therefore, the W2EF, PAD2EF and UIOEF modelling approaches are proposed, simulated and tested in a wave tank. The experimental data showed a high accordance to the estimations of the W2EF, PAD2EF and UIOEF methods. However, the application scenarios of these approaches vary, as shown below:

- The W2EF method in Eqs. (14) and (15) gives reasonably accurate estimation of the excitation force based on the conditions: (i) the incident wave is linear; (ii) the radiated wave due to the PAWEC motion is small compared to the incident wave; (iii) wave elevation measurement and its precise prediction are accessible.

- The PAD2EF approach in Eq. (22) can provide good estimation of the excitation force if the following conditions are satisfied: (i) the measurements of pressure, acceleration and displacement are available and (ii) the fluid viscous force is negligible.

- The UIOEF strategy in Eqs. (37) and (38) only depends on the displacement measurement and can provide precise estimation of the excitation force and the velocity. But the mechanical friction and fluid viscous forces cannot be decoupled from the excitation force estimation.

The UIOEF method shows great potential for the real-time power maximisation control since the measurement system is so simple and the UIO technology is flexible to apply. For off-shore application, the PAD2EF method may be more practical than the W2EF approach. The PAD2EF sensing system seems more complex than the W2EF sensing system. However, the real-time wave elevation measurement is very difficult to achieve whilst the pressure, displacement and acceleration are easy to measure.

In this study, the PTO force is not considered. When the PAWEC motion amplitude is small, the hydrodyanmic-control coupling process is linear and hence the PTO force can be substracted from or superposed into the PAWEC motion equation for dynamic/control study. Unfortunately, resent preliminary work reveals that well-designed control strategies can attempt to enhance the non-linearity of wave-buoy interaction [27, 42]. Ongoing work focuses on real-time control implementation in which the PTO force is regulated according to the excitation force estimates for the purpose of PAWEC power maximisation control.

Acknowledgment

Bingyong Guo, Siya Jin and Jianglin Lan thank the China Scholarship Council and the University of Hull for joint scholarships. Thanks are expressed to Professor Dan Parsons, Dr Stuart McLelland and Mr Brendan Murphy of the School of Environmental Sciences for their help and supervision in using the Hull University wave tank.

Appendix

The buoy dimensions were: radius $r = 0.15$ m, height $b = 0.56$ m, draft $d = 0.28$ m, mass $M = 19.79$ kg, water density $\rho = 1000$ kg/m^3, gravity constant $g = 9.81$ N/kg, hydrostatic stiffness $k_{hs} = 693.43$ N/m and added mass at infinite frequency $A_\infty = 6.58$ kg.

The system matrices of the W2EF system in Eqs. (14) and (15) were:

$$A_e = \begin{bmatrix} -0.234 & 1.818 & 0.530 & -0.554 & -0.314 & -0.054 \\ -1.818 & -0.900 & -3.043 & 1.082 & 0.861 & 0.130 \\ 0.530 & 3.044 & -1.798 & 4.233 & 1.553 & 0.306 \\ 0.554 & 1.082 & -4.233 & -2.688 & -5.096 & -0.480 \\ -0.314 & -0.861 & 1.553 & 5.096 & -3.590 & -3.064 \\ 0.054 & 0.130 & -0.306 & -0.480 & 3.064 & -0.157 \end{bmatrix}, \quad (41)$$

$$B_e = \begin{bmatrix} 164.34 & 251.36 & -236.52 & -175.67 & 114.01 & -18.71 \end{bmatrix}^T, \quad (42)$$

$$C_e = \begin{bmatrix} 1.6434 & -2.5136 & -2.3652 & 1.7567 & 1.1401 & 0.1871. \end{bmatrix}. \quad (43)$$

The system matrices for the identified radiation subsystem in Eqs. (20) and (21) were:

$$A_r = \begin{bmatrix} -3.1848 & -4.3372 & -3.1009 \\ 4.3372 & -0.0875 & -0.3882 \\ 3.1009 & -0.3882 & -2.8499 \end{bmatrix}, \quad (44)$$

$$B_r = \begin{bmatrix} -40.6964 & 5.9737 & 16.2722 \end{bmatrix}^T, \quad (45)$$

$$C_r = \begin{bmatrix} -0.4070 & -0.0597 & -0.1627 \end{bmatrix}. \quad (46)$$

The parameters of the BPF in Eq. (23) were: $\omega_c = 8\pi$ rad/s, $A_{bpf} = 2433$ and $Q_{bpf} = 100$.

The system matrices of the UIO in Eqs. (37) and (37) were:

$$P = \begin{bmatrix} -0.57 & 9.01 & 0 & 0 & 0 & 0 \\ -27.09 & -39.1 & 0.02 & 0.02 & 0.01 & 0.04 \\ -3.24 & -0.13 & -3.18 & -4.34 & -3.1 & 0 \\ -0.95 & 0.43 & 4.34 & -0.09 & -0.39 & 0 \\ 0.2 & -1.62 & 3.10 & -0.39 & -2.85 & 0 \\ -32856 & -242450 & 0 & 0 & 0 & 0 \end{bmatrix}, \quad (47)$$

$$G = \begin{bmatrix} 0 & 0.0379 & 0 & 0 & 0 & 0 \end{bmatrix}^T, \quad (48)$$

$$L = \begin{bmatrix} 357.52 & 7881.9 & 73.80 & -158.04 & -244.25 & -9183200 \end{bmatrix}^T, \quad (49)$$

$$Q = \begin{bmatrix} -8.01 & 39.1 & -40.57 & 5.55 & 17.89 & 242450 \end{bmatrix}^T. \quad (50)$$

To note: The feedback gains of the UIO were large and sensitive to measurement noise. It is due to the system property since the magnitude of the displacement $z(t)$ is 10^{-2} and the magnitude of the excitation force $F_e(t)$ is 10. Thus this is a numerical stiffness or conditioning problem with varying ratio 10^3. In this study a low-pass filter were applied to the displacement measurement to attenuate the noise.

References

[1] M. McCormick, Ocean wave energy conversion, Wiley-Interscience, New York, 1981.

[2] A. Falcão, Wave energy utilization: A review of the technologies, Renew. Sustainable Energy Rev. 14 (3) (2010) 899–918.

[3] B. Drew, A. Plummer, M. N. Sahinkaya, A review of wave energy converter technology, P. I. Mech. A-J Pow. 223 (8) (2009) 887–902.

[4] A. Clément, P. McCullen, A. Falcão, A. Fiorentino, F. Gardner, K. Hammarlund, G. Lemonis, T. Lewis, K. Nielsen, S. Petroncini, et al., Wave energy in Europe: current status and perspectives, Renew. Sust. Energ. Rev. 6 (5) (2002) 405–431.

[5] J. V. Ringwood, G. Bacelli, F. Fusco, Energy-maximizing control of wave-energy converters: The development of control system technology to optimize their operation, IEEE Control Systems 34 (5) (2014) 30–55.

[6] S. Salter, Power conversion systems for ducks, in: Proc. of the International Conference on Future Energy Concepts, Vol. 1, 1979, pp. 100–108.

[7] K. Budal, J. Falnes, Optimum operation of improved wave-power converter, Mar. Sci. Commun. 3 (2) (1977) 133–150.

[8] A. Babarit, M. Guglielmi, A. H. Clément, Declutching control of a wave energy converter, Ocean Eng. 36 (12) (2009) 1015–1024.

[9] G. Li, M. R. Belmont, Model predictive control of sea wave energy converters–part i: A convex approach for the case of a single device, Renew. Energy 69 (2014) 453–463.

[10] G. Li, M. R. Belmont, Model predictive control of sea wave energy converters–part ii: The case of an array of devices, Renew. Energy 68 (2014) 540–549.

[11] J. N. Newman, The exciting forces on fixed bodies in waves, Journal of Ship Research 4 (1962) 10–17.

[12] M. Greenhow, S. White, Optimal heave motion of some axisymmetric wave energy devices in sinusoidal waves, Appl. Ocean Res. 19 (3-4) (1997) 141–159.

[13] A. Babarit, J. Hals, M. Muliawan, A. Kurniawan, T. Moan, J. Krokstad, Numerical benchmarking study of a selection of wave energy converters, Renew. Energy 41 (2012) 44–63.

[14] Z. Yu, J. Falnes, State-space modelling of a vertical cylinder in heave, Appl. Ocean Res. 17 (5) (1995) 265–275.

[15] J. Falnes, On non-causal impulse response functions related to propagating water waves, Appl. Ocean Res. 17 (6) (1995) 379–389.

[16] G. Bacelli, R. G. Coe, D. Patterson, D. Wilson, System identification of a heaving point absorber: Design of experiment and device modeling, Energies 10 (4) (2017) 472.

[17] S. Giorgi, J. Davidson, J. Ringwood, Identification of nonlinear excitation force kernels using numerical wave tank experiments, in: Proc. EWTEC, Nantes, France, 2015, pp. 09C1–1–1–09C1–1–10.

[18] B. A. Ling, Real-time estimation and prediction of wave excitation forces for wave energy control applications, Master's thesis, Mechanical Engineering, Oregon State University (2015).

[19] O. Abdelkhalik, S. Zou, G. Bacelli, R. D. Robinett, D. G. Wilson, R. G. Coe, Estimation of excitation force on wave energy converters using pressure measurements for feedback control, in: Proc. OCEANS MTS/IEEE Monterey, IEEE, 2016, pp. 1–6.

[20] G. Bacelli, R. G. Coe, State estimation for wave energy converters, Tech. rep., Sandia National Laboratories (SNL-NM), Albuquerque, NM (United States) (2017).

[21] M. Abdelrahman, R. Patton, B. Guo, J. Lan, Estimation of wave excitation force for wave energy converters, in: Proc. SysTol, IEEE, 2016, pp. 654–659.

[22] F. Fusco, J. V. Ringwood, Short-term wave forecasting for real-time control of wave energy converters, IEEE Trans. Sustain. Energy 1 (2) (2010) 99–106.

[23] M. Ge, E. C. Kerrigan, Short-term ocean wave forecasting using an autoregressive moving average model, in: Proc. UKACC, IEEE, 2016, pp. 1–6.

[24] J. Falnes, Ocean waves and oscillating systems: linear interactions including wave-energy extraction, Cambridge University Press, 2002.

[25] J. N. Newman, Marine hydrodynamics, MIT Press, 1977.

[26] W. Cummins, The impulse response function and ship motions, Tech. rep., DTIC Document (1962).

[27] G. Giorgi, J. V. Ringwood, Implementation of latching control in a numerical wave tank with regular waves, Journal of Ocean Engineering and Marine Energy 2 (2) (2016) 211–226.

[28] A. Babarit, G. Delhommeau, Theoretical and numerical aspects of the open source bem solver nemoh, in: Proc. EWTEC, Nantes, France, 2015, pp. 1–10.

[29] A. Roessling, J. Ringwood, Finite order approximations to radiation forces for wave energy applications, Renewable Energies Offshore (2015) 359–366.

[30] R. Taghipour, T. Perez, T. Moan, Hybrid frequency–time domain models for dynamic response analysis of marine structures, Ocean Eng. 35 (7) (2008) 685–705.

[31] S.-Y. Kung, A new identification and model reduction algorithm via singular value decomposition, in: Proc. ACSC, IEEE, 1978, pp. 705–714.

[32] M. Safonov, R. Chiang, A schur method for balanced model reduction, in: Proc. ACC, IEEE, 1988, pp. 1036–1040.

[33] J. R. Halliday, D. G. Dorrell, A. R. Wood, An application of the Fast Fourier Transform to the short-term prediction of sea wave behaviour, Renew. Energy 36 (6) (2011) 1685–1692.

[34] B. Fischer, P. Kracht, S. Perez-Becker, Online-algorithm using adaptive filters for short-term wave prediction and its implementation, in: Proc. 4th Inter. Conf. Ocean Energy, Vol. 1719, Dublin, Ireland, 2012, pp. 1–6.

[35] W. J. Pierson, L. Moskowitz, A proposed spectral form for fully developed wind seas based on the similarity theory of SA Kitaigorodskii, J. Geophys. Res. 69 (24) (1964) 5181–5190.

[36] J. Lan, R. J. Patton, Integrated design of robust fault estimation and fault-tolerant control for linear systems, in: Proc. CDC, IEEE, 2015, pp. 5105–5110.

[37] J. Lan, R. J. Patton, Integrated design of fault-tolerant control for nonlinear systems based on fault estimation and T-S fuzzy modelling, IEEE Trans. Fuzzy Syst. 25 (5) (2017) 1141–1154.

[38] Met Office, Exert,UK, National Meteorological Library and Archive Faxt sheet 6-The Beaufort Scale, 1st Edition, accessed: 2017-07-15.

[39] B. Guo, R. Patton, S. Jin, J. Gilbert, D. Parsons, Nonlinear modeling and verification of a heaving point absorber for wave energy conversion, IEEE Trans. Sustain. Energy 9 (1) (2018) 453–461.

[40] B. Guo, R. J. Patton, Non-linear viscous and friction effects on a heaving point absorber dynamics and latching control performance, in: Proc. IFAC World Congress, Elsevier, 2017, pp. 15657–15662.

[41] F. Fusco, J. Ringwood, A model for the sensitivity of non-causal control of wave energy converters to wave excitation force prediction errors, in: Proc. EWTEC, Southampton, UK, 2011, pp. 1–10.

[42] R. Genest, J. Davidson, J. V. Ringwood, Adaptive control of a wave energy converter, IEEE Trans. Sustain. Energydoi:10.1109/TSTE.2018.2798921.